Chapter 5

Application & Implementation

The world is what it is and I am what I am… This out there and this in me, all this, everything, the result of inexplicable forces. A chaos whose order is beyond comprehension

Henry Miller, Black Spring

Electrostatic potential was shown to dramatically affect the bifurcation sequence of chaotic bubbling. An increase in electrostatic potential caused an increase in the average bubbling at a constant flow rate. This has provocative implications wherein the effect of electrostatic potential can be harnessed to optimize and control the entire bubbling phenomena. The emphasis in this research was on closed loop control enhancements to process performance.

5.1. Periodicity identification

The bubbling periodicity identification was the initial step to controlling bubbling. This identification was to be done in real time so that dynamic calculations could be utilized to control the bubbling.

5.1.1. Statistical modeling

An initial approach was modeling the bubbling periodicities as a function of the frequency distribution of the periods of formation using various regression techniques. (Sarnobat & Hines, 1999). The results were not satisfactory because of the non-linearity and extreme sensitivity of the bubbling process to perturbations, as against the least squares approach adopted by most of the regression analysis. A sample of the model performance is shown in **figure 5.1**. The model performance degraded when the system changed from higher periodicities to lower ones. Near chaotic conditions, the model could not discriminate between any of the regimes.

5.1.2. Neural network models

It was found that power spectrum analysis could be used to extract the significant information (section 4.2). The fundamental peak gives the average frequency of bubbling (say x) and peaks observed at 0.75x, 0.5x, 0.25x give information about the periodicity regimes of the bubbling (figures 4.4, 4.7, 4.10, 4.13). A non-zero peak height at 0.5x suggests period-2 and a peak at 0.25x indicate period-4. The peak at 0.75x is a harmonic of frequencies at 0.25x, but also gives a qualitative indication about the existence of chaos. The peak heights of these peaks along with the average bubbling frequency are all that are required to characterize the bubbling periodicity. A neural network was constructed to map periodicity regimes of bubbling (Sarnobat and co-workers, 1999). The neural network was designed to have 5 inputs and one output. Four of the five inputs were the peak heights at multiples of 1x, 0.75x, 0.5x, 0.25x, where x is the fundamental frequency in the power spectrum distribution of the time series. The fifth input was the value of the fundamental frequency itself. The neural network had one output, which was the periodicity of the system. A periodicity of 16 was assigned to the class when the system was in deterministic chaos. A Kohonen based neural network was used and the training was conducted

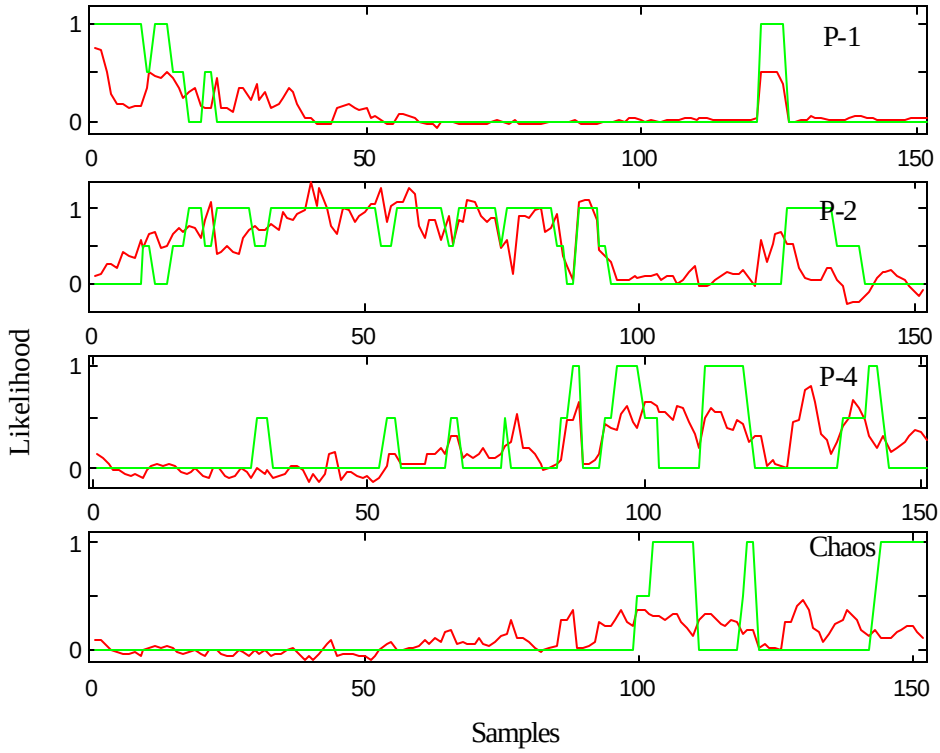

Figure 5.1. Performance of numerical model using partial least squares. Input data are the frequency distribution of the periodicity and the output is a 'state' vector, which indicates the likelihood of the bubbling regime. Each of the periods was assigned a 'likelihood' between 0-1 which indicated the extent to which the system corresponded to that state. (The green line indicates the target and the red line is the estimated state)

with linear vector quantization, (Tsoukalas & Uhrig, 1996; Sarnobat & co-workers, 1999). The performance of the neural network model is shown in **figure 5.2**. The model performance was found to be satisfactory, but implementation in LabView for real time calculations was difficult. Also for the neural network large amounts of training data were required and the model would only be valid if the operating regimes were all comprehensively represented in the training data. This was a big factor in considering other techniques for real time identification.

5.1.3. Periodicity pattern detector

An important constraint on the real time periodicity identification is the adaptability of the algorithm to LabView implementation. A real time simultaneous input/output *vi* was designed to calculate the periods of formation. This was a software timed data acquisition and hence all the calculations were done within a 10ms loop between data points. The disadvantage of this method was that any memory usage of by the operating system reflected in the timing loops being longer than the 10ms. This caused a outliers in the zero-crossings because the time between zero-crossings also included the additional processing time required by LabView. The effective rate of data acquisition was 100Hz at the 'worst' operating condition, which took maximum length of time to process the data. The periods of formation were dynamically plotted as a time return map, which clearly indicated the periodicity of formation.

A simple 'pattern-identifier' routine was set up to identify the bubbling regime. It was based on the observation that regular patterns are formed in periodic regimes and in chaos no pattern can be detected. For period-1 formation, every bubble is of the same size, for period-2 every third bubble and for period-4, every fourth bubble. In chaos none of the bubbles form a pattern. A target array of every second, third & fourth bubble set up. The value of the period of formation of the current bubble was subtracted from each of the array elements and the averaged differences are compared against a tolerance. A moving window based approach was used keeping

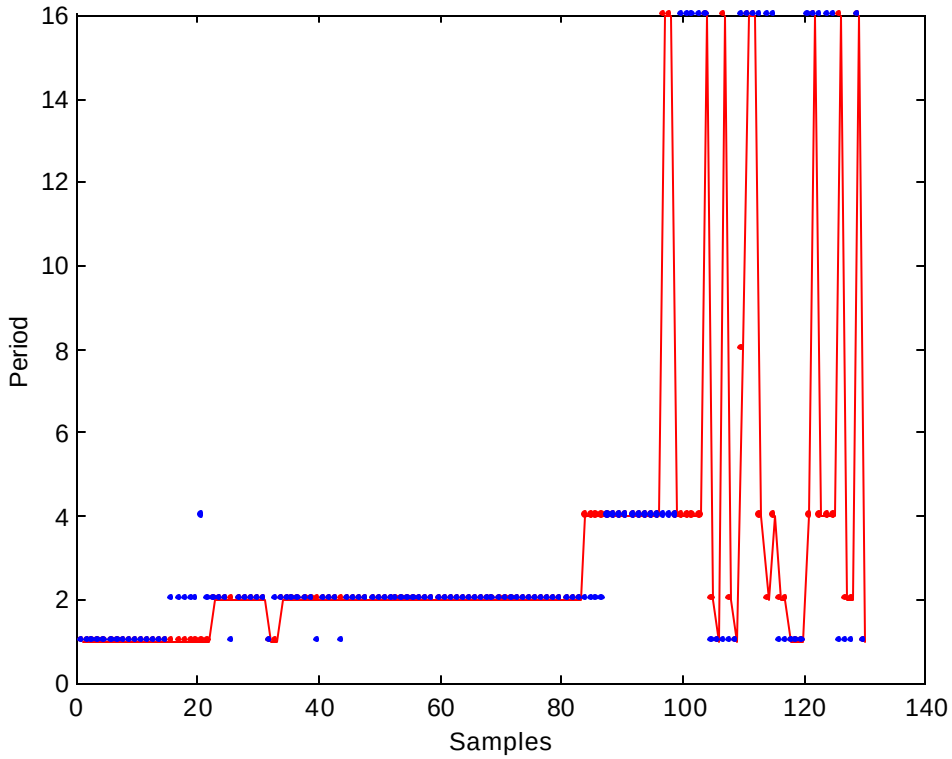

Figure 5.2. Neural network performance for identifying the periodicity of bubbling. A Kohonen map was used and the network trained by linear vector quantization. The inputs were the fundamental peak heights extracted from the power spectrum distribution and the average bubbling frequency. (The red dots indicate the target and the blue dots indicate the estimated state).

{Bubble (3)-Bubble(0)}<tolerance	*{Bubble (2)-Bubble(0)}<tolerance*	*{Bubble (1)-Bubble(0)}<tolerance*	*Regime*
0	0	0	Chaos
0	0	1	?
0	1	0	Period-4
0	1	1	Period-1
1	0	0	Period-4
1	0	1	?
1	1	0	Period-2
1	1	1	Period-1

Table 5.1. Truth table for bubble regime identification (Key: Y=1, N=0)

the last 32 bubbles in the history array. Longer windows can be used to decrease the over-sensitivity of the identifier to changes in periodicity. Depending on which elements are below the tolerance, a truth table is set-up for the regimes of bubbling.

The results (**figure 5.3, 5.4**) suggest that this regime identifier can be used with confidence for detecting period-1 and period-2. But, when the bubbling regime enters period-4, the measurement error due to either computational limits reached by LabView or due to external noise, causes erratic results because this identifier compares the bubble sizes and any error will cause a misclassification of period-4.

This identifier was used for feedback control to ensure regime of bubbling. A simple P-I controller can be implemented for manipulating the flow-rate and/or voltage to achieve the required regime of bubbling. Presently this is limited by computational requirements for control into either of the regimes.

5.2. Regime targeting of bubbling with electrostatic potential

Electrostatic potential was shown to affect the frequency of bubbling in a manner similar to increasing the flow rate. In the frequency plot of figure 4.34, it can be seen that for a single

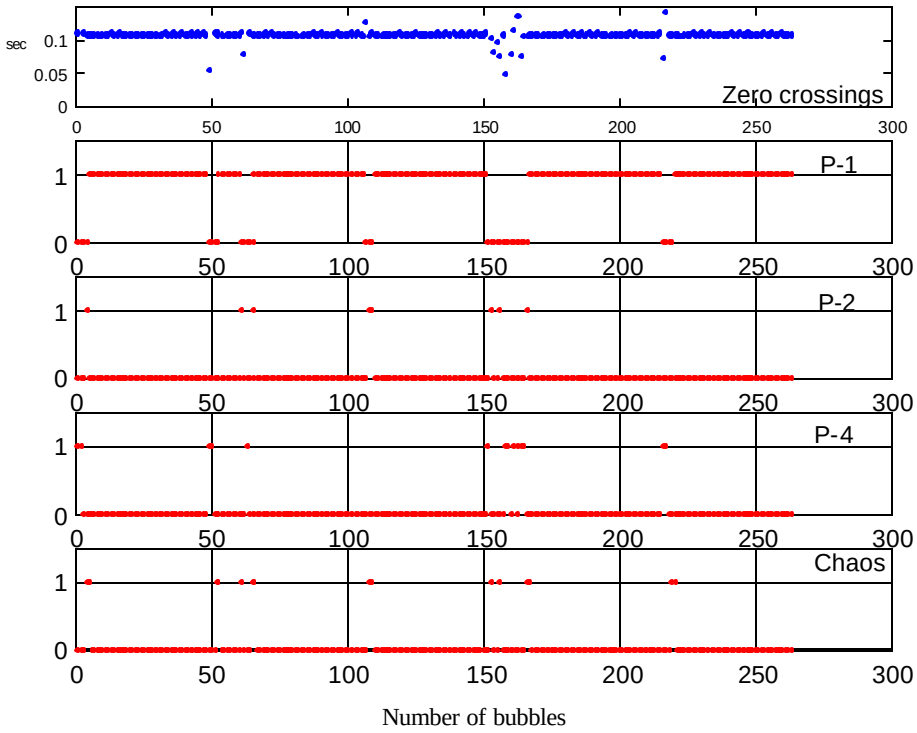

Figure 5.3. Period-1 identification with periodicity pattern identifier. Blue plot is the zero-crossings (in units of seconds), plotted against the bubble indices. The red plots are the flags for each of the periodicities. This plot shows that the identifier captures period-1 satisfactorily (P-1).

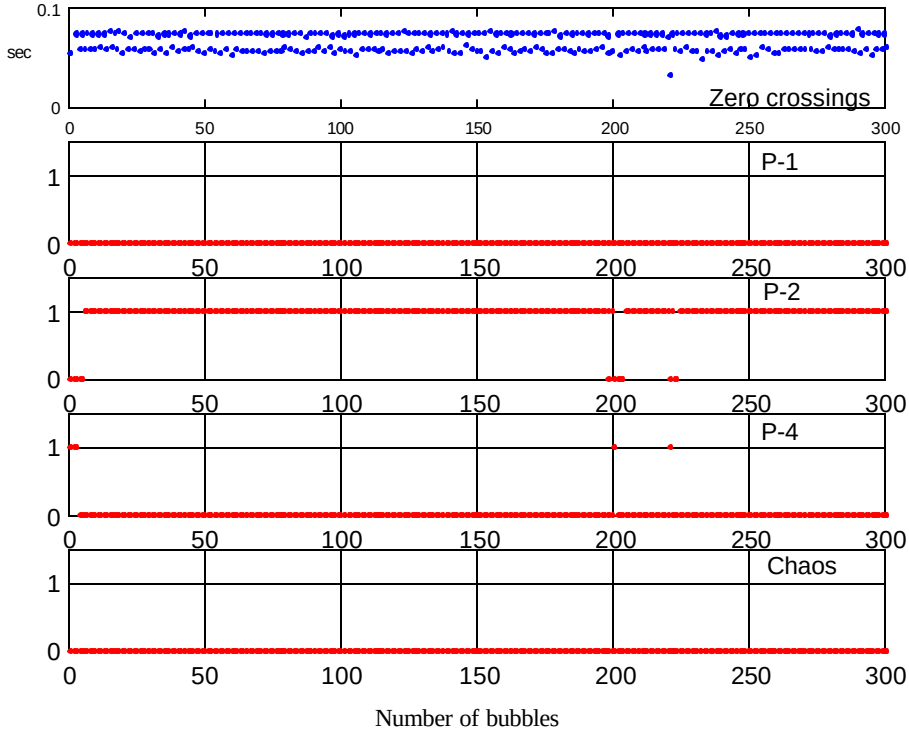

Figure 5.4. Period-2 identification with periodicity pattern identifier. Blue plot is the zero-crossings (units in seconds),plotted against the bubble indices. The red plots are the flags for each of the periodicities. This plot shows that the identifier captures period-2 satisfactorily (P-2).

frequency of bubbling, an operating line can be determined. This suggests that voltage and flow can be used in tandem to maintain constant bubbling frequency. An increase in flow rate can be compensated by a corresponding decrease in electrostatic potential, or vice versa.

A simple PI-controller loop was used with voltage as the manipulated variable, flow rate as the disturbance and the average bubbling frequency as the process variable to be held at a set-point. The average bubbling frequency was calculated by taking the mean of the previous 20 bubbles. The control moves were implemented after multiples of 20 bubbles (~1s) to give the system time to stabilize before implementing the next control move. Results are shown in **figures 5.5-5.7**.

Figure 5.5 (a) shows the response of the system to a gradual increase in the disturbance (flow rate). The period for formation, manipulated variable (electrostatic potential) and flow-rate are plotted against the number of bubbles. Before the disturbance was introduced into the system, the system was at a steady period 1 bubbling with the electrostatic potential at 10kV. The flow rate was gradually varied in a series of small increments from 200cc/min to 420 cc/min. The set point was set to the average bubbling frequency before the disturbance was introduced. The aim was to get the controller to manipulate voltage to match the bubbling frequency before the disturbance was injected.

From figure 5.5, it can be seen that the controller steps down the voltage so maintain a constant bubbling period of formation (0.05s). The plot for the flow rate is noisy on the right hand side because the flow rate varies as the pressure at the nozzle varies with the formation of each bubble. Figure 5.5 (b) shows the return maps before and after the disturbance. Before the disturbance is injected, the system is in a 'noisy' period-1. After the controller has compensated for the disturbance, the bubbling frequency is maintained at the set point, but now the system is into a noisy period-4.

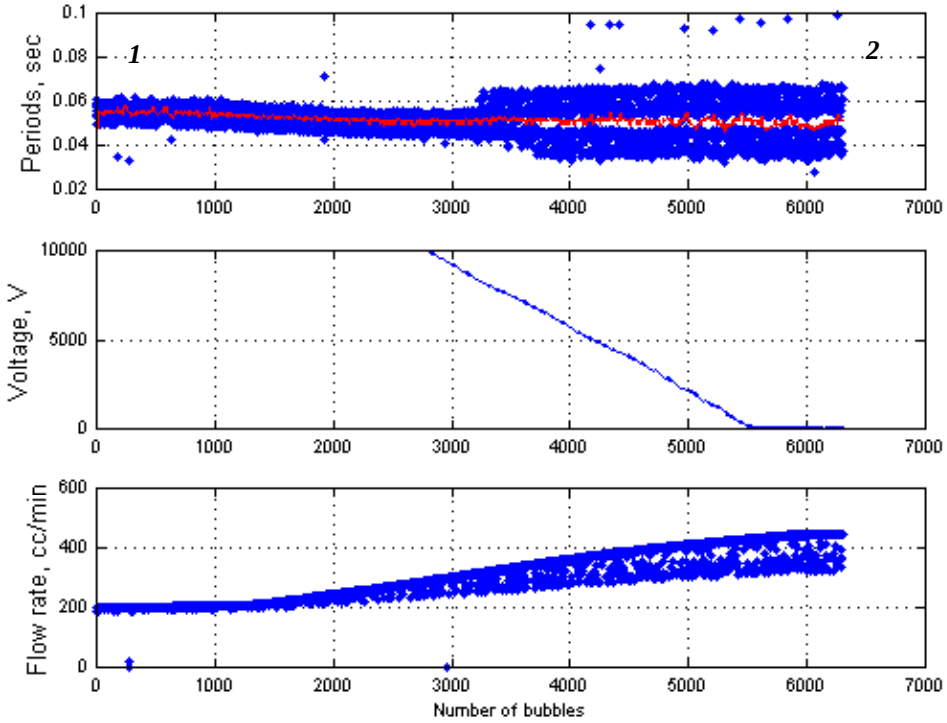

(a)

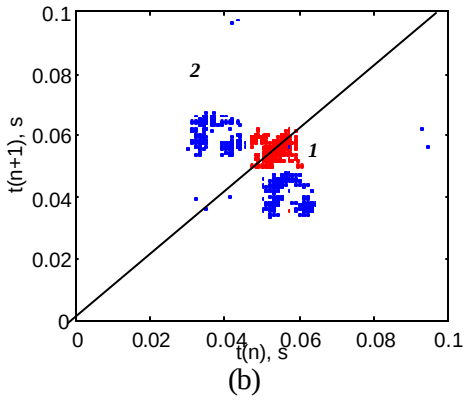

(b)

Figure 5.5. (a) An drift of 220cc/min in the disturbance (flow-rate), compensated by voltage to track a set point of constant bubbling frequency (0.05s). (b)System goes from noisy period-1 at state '1' to period-4 at state'2'

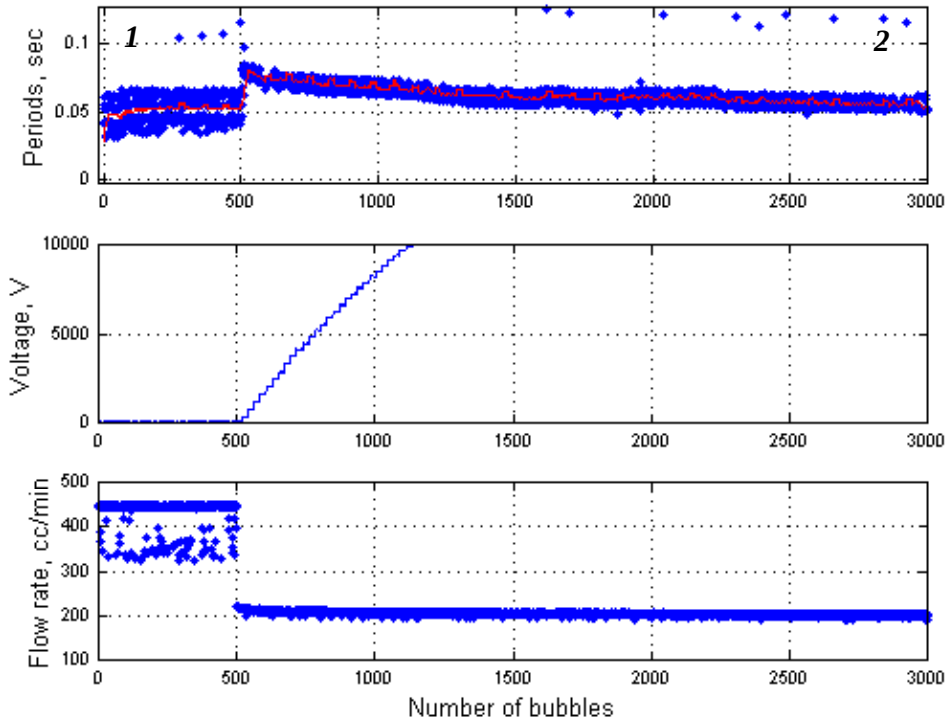

(a)

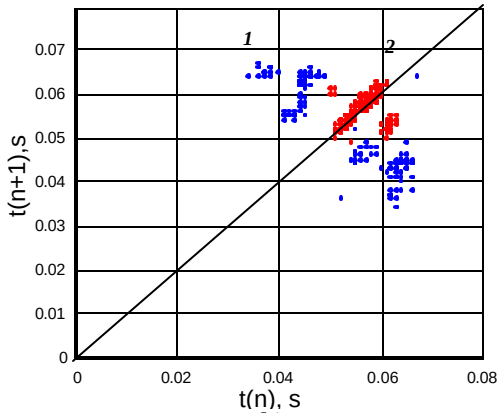

(b)

Figure 5.6. (a) Negative step change of 235cc/min in disturbance (flow rate) tracked by voltage for a set point of 0.05s. (b) System goes from period-4 at state '1' to noisy period-1 at state'2'.

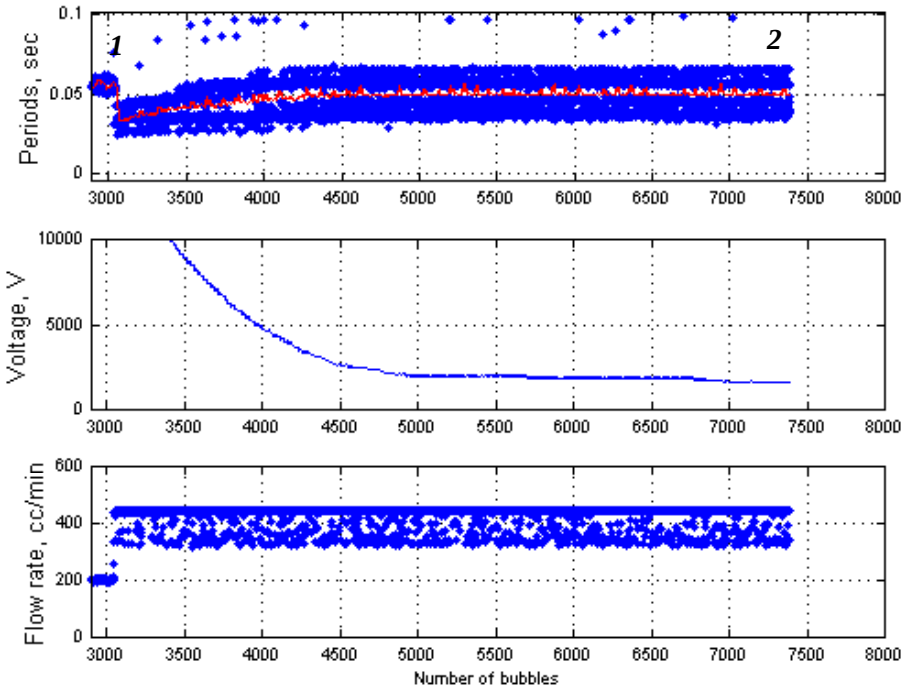

(a)

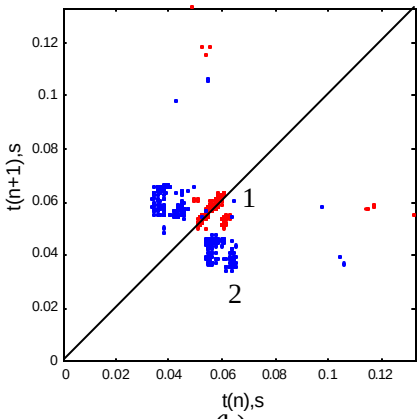

(b)

Figure 5.7. (a) Positive step change of 220cc/min in disturbance (flow rate) tracked by voltage for a set point of 0.05s (b) System goes from noisy period-1 at state '1' to period-4 at state'2'.

Figure 5.6 illustrates the effect of a negative step change of 235 cc/min in the disturbance. The controller compensates the disturbance and in effect the system goes from a period-4 to a noisy period-1.

Figure 5.7 illustrates the effect of a positive step change of 220 cc/min in the disturbance. The controller action maintains the set point of 0.05s, but changes the periodicity of the system from a period-1 into period-4.

In figures 5.5-5.7, outliers are observed on the plot, which shows the zero-crossings. These outliers (at ~0.9-1.0s) are actually the formation times of two bubbles, which are caught because of a computing limitation of LabView. These do not cause a control loop problem as moving window approach is adopted and an average past bubble period is used as the process variable. For the runs shown in the figures 5.5-5.7, a moving window of 20 bubbles was found to give satisfactory results.

5.3. OGY Control

The slow control regime targeting method described in section 5.2, demonstrates the effect of voltage and suggests that electrostatic potential can be used for control of individual bubbles at a higher frequency.

5.3.1. Calculations

The crucial step for control is the extraction of information about system stability from the time return maps. This is because all the constants in the control law are calculated from the values of the stable and unstable manifolds and their corresponding eigenvalues, which in turn are

obtained from time return maps. The development of the OGY control algorithm has been presented in an earlier section (chapter 2).

There are four aspects to this calculation

1. Identifying the unstable fixed-point
2. Calculating the manifold directions
3. Computing the eigenvalues
4. Shift vector determination

The first two steps are shown in **figure 5.8-5.9**.

5.3.1.1. Identifying the unstable fixed-point

The unstable fixed-point can be thought of as a periodic trajectory onto which the system is to be stablized. On the time return map, (which can be thought of as pseudo-phase space), the point moves along the stable manifold, mapping to the fixed-point, and continues to map to the fixed-point, until a perturbation causes it to continue along the unstable manifold to complete the sequence. For a chaotic attractor, each of the properties is necessary and sufficient. This means that all points which map to then selves are fixed-points and all fixed-points map to themselves.

5.3.1.2. Calculating the manifolds

To calculate the stable and unstable manifolds, various methods have been suggested. A least square fitting method has been suggested in Cheng (1996), in which the mapping matrix M is calculated by least square approximation of the map data. This method though is fraught with errors and as the chaotic system is highly sensitive to the smallest

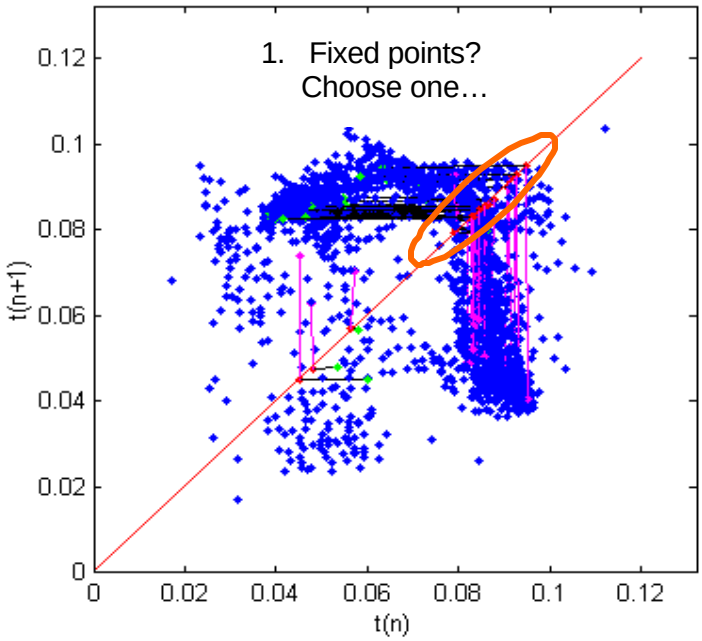

Figure 5.8. Sorting fixed points on the 45º line on the time return map to find a true fixed-point. (Flow-rate: 443 cc/min, voltage:10,000V)

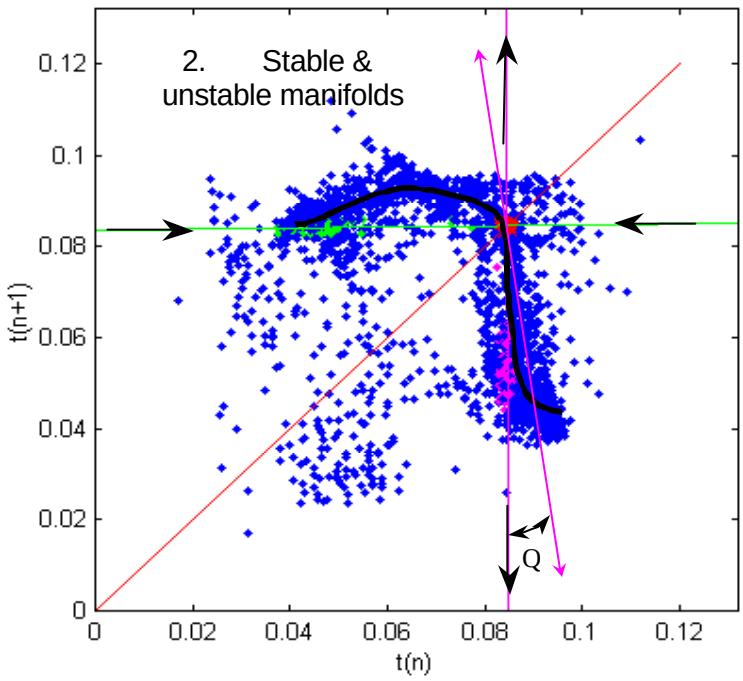

Figure 5.9. Identifying the stable and unstable manifold directions. The angle Θ denotes the deviation of the calculated unstable manifold from the true unstable manifold, which is along the tangent to the attractor at the fixed point. The black line approximates the shape of the true attractor. (Flow-rate: 443 cc/min, voltage:10,000V)

perturbations (such as noise), the effectiveness of this method is greatly reduced. Another method suggested by Cheng (1996), uses cluster analysis to calculate the manifolds.

In this method, like other conventional fixed-point calculation approaches, a small tolerance is chosen to approximate a region around the fixed-point. Then the points, which map to that region are selected and the manifolds calculated. It was observed that in some cases the points map to the fixed-point, jump within the approximated tolerance and then jump out along the unstable manifold. In such cases, the movement of the fixed-point within the tolerance is neglected. But the location of the fixed-point has to be approximated first. This is tricky because the system has to 'hit' the fixed-point multiple times to be sure that it is the fixed-point. In experimental trials, due to presence of system noise, the chaotic system may map to the neighborhood of the unstable fixed-point a number of times before mapping to the fixed-point itself. A comprehensive dataset is required before enough information about the fixed-point location is acquired.

The direction of the unstable manifold is the tangent to the chaotic attractor at the fixed-point location (figure 5.9). Identification of the manifolds from experimental data is usually different from the direction of the manifold calculated from analysis of the time return map. To compensate from the error in manifold direction, the calculated unstable manifold direction was swept through an angle of 15º on either side to search the control law solution space.

5.3.1.3.Calculating the eigenvalues

By knowing the manifold directions and hence the eigenvectors, one can calculate the corresponding eigenvalues based on the following procedure, (taken from Cheng, 1996). Consider two consecutive mapping points going to the fixed-point.

$$p_1 = [t_n \quad t_{n+1}]$$
$$p_2 = [t_{n+1} \quad t_{n+2}]$$

The slope between these points is:

$$m = \frac{t_{n+2} - t_{n+1}}{t_{n+1} - t_n}$$

Since they are located on the same eigenvector, the generalized solution for mapping points can be written in the form:

$$t_{n+k} = \frac{l^2 t_n - l t_n}{l t_n - t_{n+1}} = \frac{l(l-1)}{(l-1)}$$

Taking the limit as $l \to 0$, the eigenvalues around the fixed-point are equal to the slopes of the eigenvectors by L'Hospitals rule:

$$m = \begin{cases} l & l \neq 1 \\ l & l = 1 \end{cases}$$

The following algorithm was used to calculate the fixed-point and the manifolds.

1. After studying time return maps, a MATLAB™ routine was written to sort the points which map within a certain distance of each other. A single fixed-point was isolated by visual inspection of the walk-in states. (Figure 5.8)
2. After choosing a tolerance around this fixed-point, points that mapped to this region were determined and the stable direction calculated as an average of many directions identified (figure 5.9).
3. Unstable manifolds were approximated as the direction along which maximum numbers of points leave the fixed-point location. This direction was then varied through 15º on either side of the approximated unstable manifold direction to compensate for the error in approximation.

5.3.1.4.Shift vector

The shift vector is a measure of how much a unit change in the perturbation changes the location of the fixed point. It is calculated by calculating the fixed-point location from return maps at corresponding to two different conditions of the control variable and then observing the change in the fixed point. For the present experiment, the two return maps were plotted at 9500V and 10500V giving an effective perturbation of 1000v to the system. The change in the fixed point was found to be 0.001s. Thus the change in the return map per unit volt increase in the electrostatic potential is 1e-5s.

The OGY control algorithm in its final form is:

$$\Delta p = \frac{l_u}{l_u - 1}\frac{f_u^T \Delta x_n}{f_u^T s} = c\Delta x_n$$

and is implemented as

$$\Delta p = c_1\left(c_2\Delta x_1 + c_3\Delta x_2\right) = c\Delta x_n$$

5.3.2. Results

Choice of the bubbling regime was based on the following observations:

1. Control gain available with electrostatic potential was greater at higher voltages. From figure 4.34, it can be seen that the voltage gain has a non-linear behavior and changes in bubbling with unit changes in voltage are greater at higher voltages applied at the nozzle.

2. From the flow rate response, it can be seen that the flow rate affects the bubbling with an order of magnitude increase over electrostatic potential. To counter the effect of flow, a

comparatively large gain in electrostatic potential is needed (which is not possible with the limitations of current equipment). Consequently the minimum flow rate needed to ensure that the system was in chaos at the operating voltage was chosen.

The goal was to bring the system back into higher periodicities, ideally to period-1. Several runs with the OGY parameters were carried out and manual tuning of the gain coefficients had to be done to ensure that the control moves were in operating limits. A scaling coefficient (c_1) of the order of 10^{-2} had to be added to get the calculated controller output to be in the permissible range of the voltage rippler which was $\pm$ 490V. For the control trial carried out in **figure 5.10** the following constants were used:

1. Base voltage: 10,000 V
2. Flow-rate: 443 cc/min
3. Controller coefficients: c_1=0.01, c_2=-6.2e5, c_3=0.084e5
4. Data acquisition rate: 100Hz

These constants were for the set of operating conditions unique to this experimental run. Time return maps and manifold calculations were carried out for every experimental run as the system information changed with every change in operating conditions.

The results of a representative OGY control attempt is shown in figure 5.10. In section (a), the system is nearly fully chaotic with no voltage being applied and with the application of electrostatic potential in (b), the system goes in to, what can be termed as, 'full-blown' chaos. Note that a remnant of a period-4 signature can be observed in (b). When the controller action is initiated at index 890 in section (c_1), it can be seen that though the system is still in chaos, the

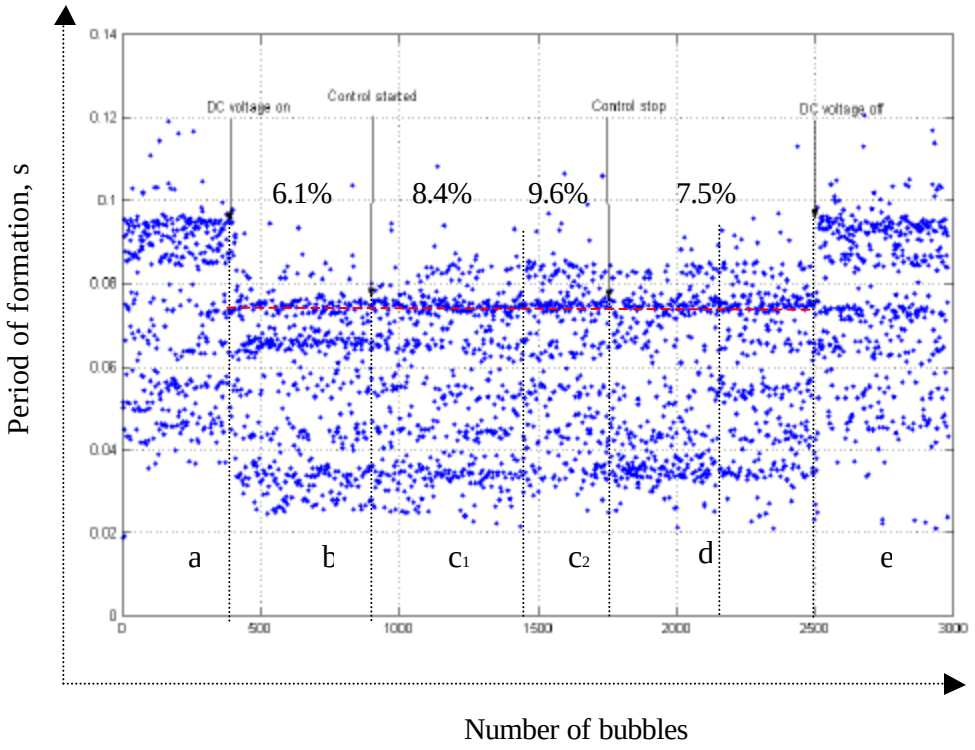

Figure 5.10. OGY control attempt with electrostatic potential as the single control variable. a) No DC voltage applied. b) 10kV DC voltage applied. c) Control initiated. d) Control stopped. e) DC voltage turned off. The red line indicates fixed-point location.

period-4 signature is less distinct. Instead an additional band is observed at the top where the system fixed-point location is calculated. In section (c_2) it can be seen that there is only one band of bubbling. This is because the OGY control moves tend to *'push'* the system on the stable manifold and the points favor dwelling on the fixed-point. The red line indicates the fixed-point location. The control was turned off at the index 1750. Even after the control is turned off, the system is seen to be in a state of entrainment in section (d) and the entrainment is lost in section (e) where appearance of additional bands is seen. The voltage was again turned off at an index of 2500.

Tight control was not observed in controlling the bubbling to a periodic state from its open-loop chaotic behavior with control turned on, but a distinct effect of the control moves on the bubbles was obvious. The effect of the control scheme is better illustrated in a frequency distribution plot (**figures 5.11-5.14**). A progressive increase in the hits on the fixed-point can be seen when the control is turned on (figures 5.12-5.13), as opposed to when there is no control (figures 5.11, 5.14). After the control is turned off (figure 5.14), the number of fixed-point hits is observed to be higher than the number before the control was turned on (figure 5.11). This can be explained by the entrainment phenomenon in which a chaotic system maintains characteristics even after the perturbations are turned off.

5.3.3. Entrainment studies

In the present control experiments, tight control was not observed. It was surmised that the controllers gain of 490 V provided by the voltage 'rippler' was not sufficient. To confirm this assumption, entrainment studies were carried out (Cheng, 1996). The response of the bubbling to a square wave of $\pm$ 490V amplitude at various frequencies was studied. No perceptible change

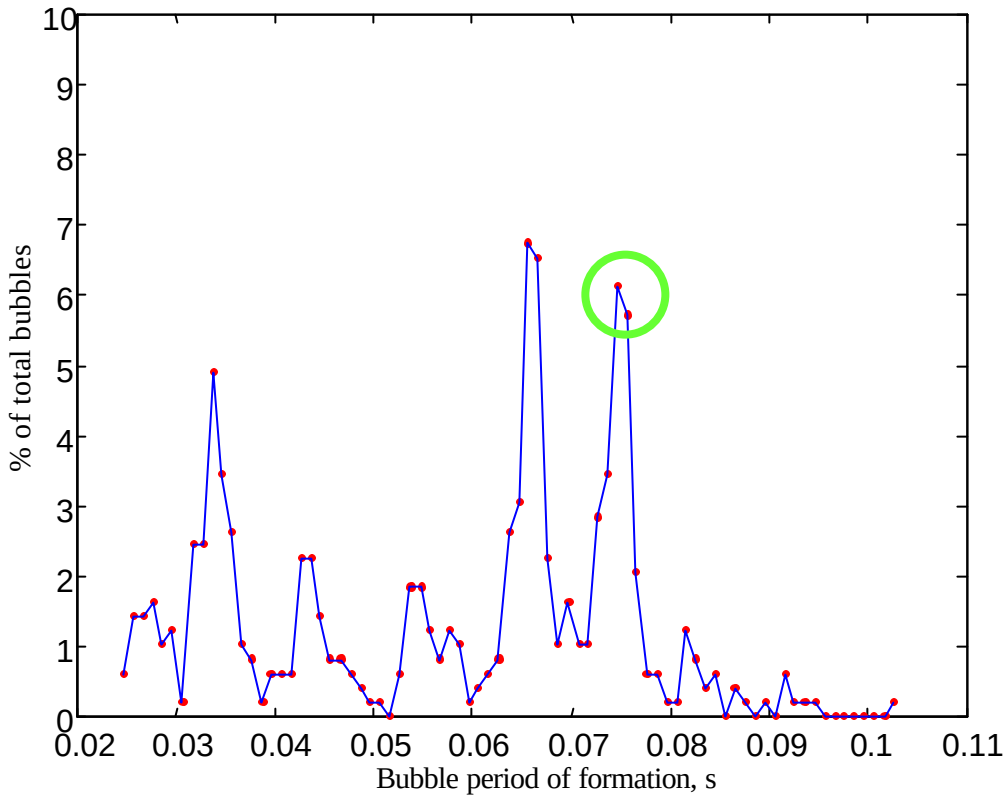

Figure 5.11. Frequency distribution of zero crossings before control is turned on (region b). Fixed point hits observed are 6.1% of the total number of bubbles

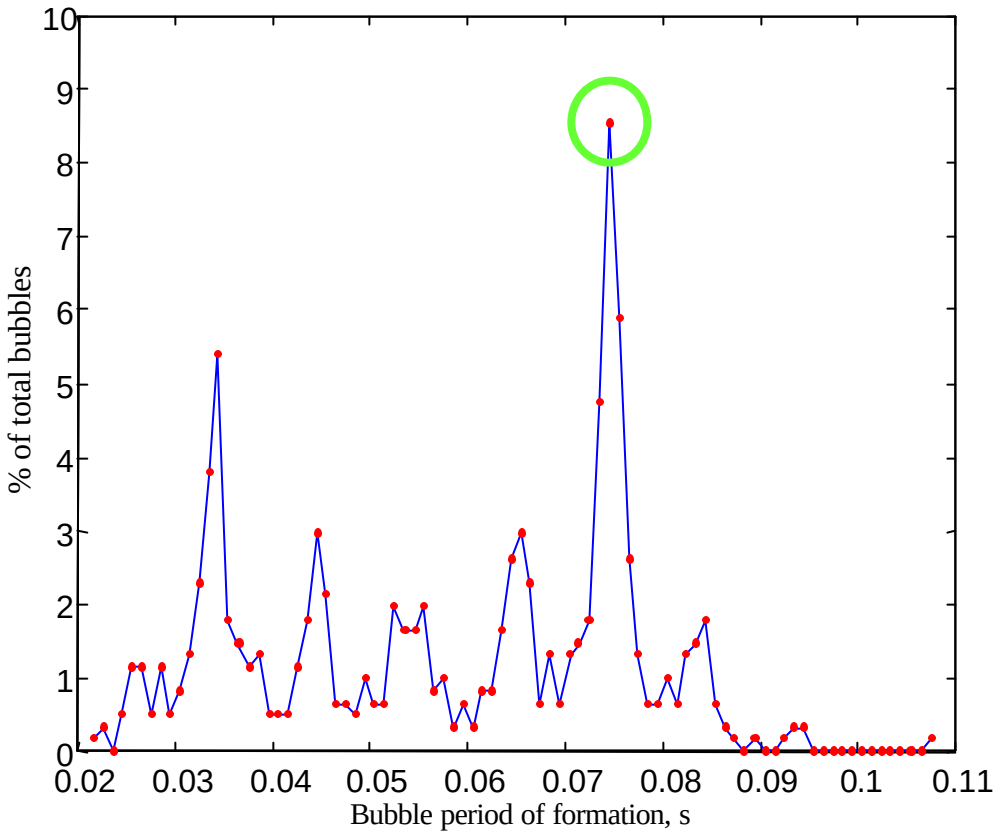

Figure 5.12. Frequency distribution of zero crossings after control is turned on (region c_1). Fixed-point hits increase to 8.4% of the total number of bubbles

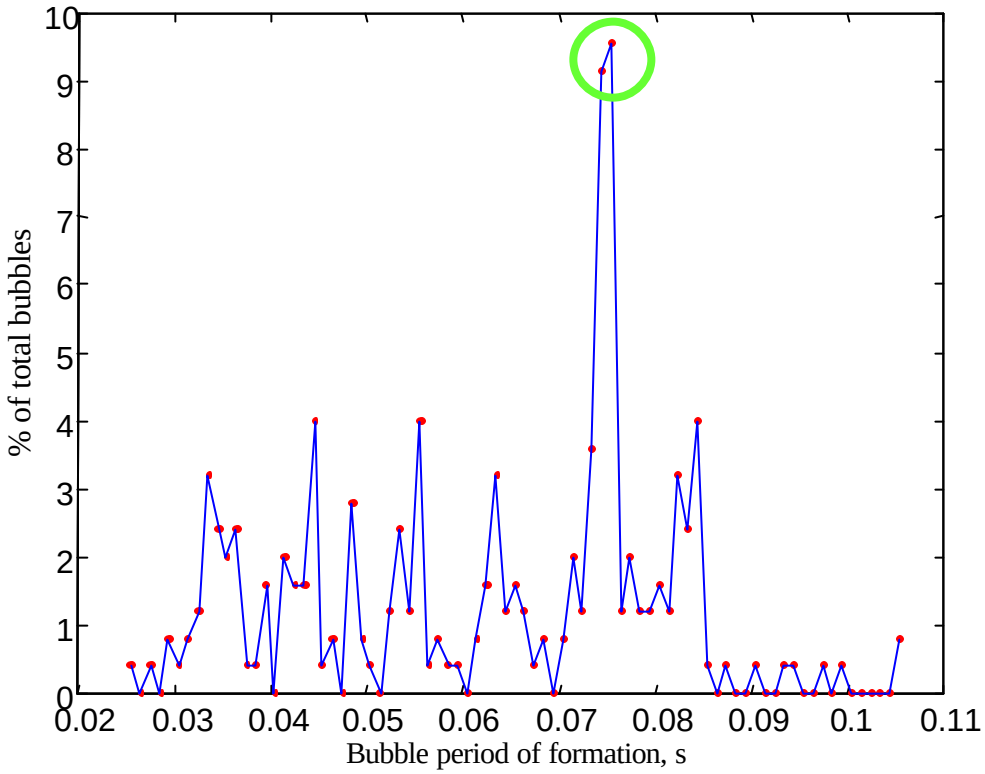

Figure 5.13. Frequency distribution of zero crossings after control is turned on (region c_2). Fixed-point hits observed increase to 9.6% of the total number of bubbles.

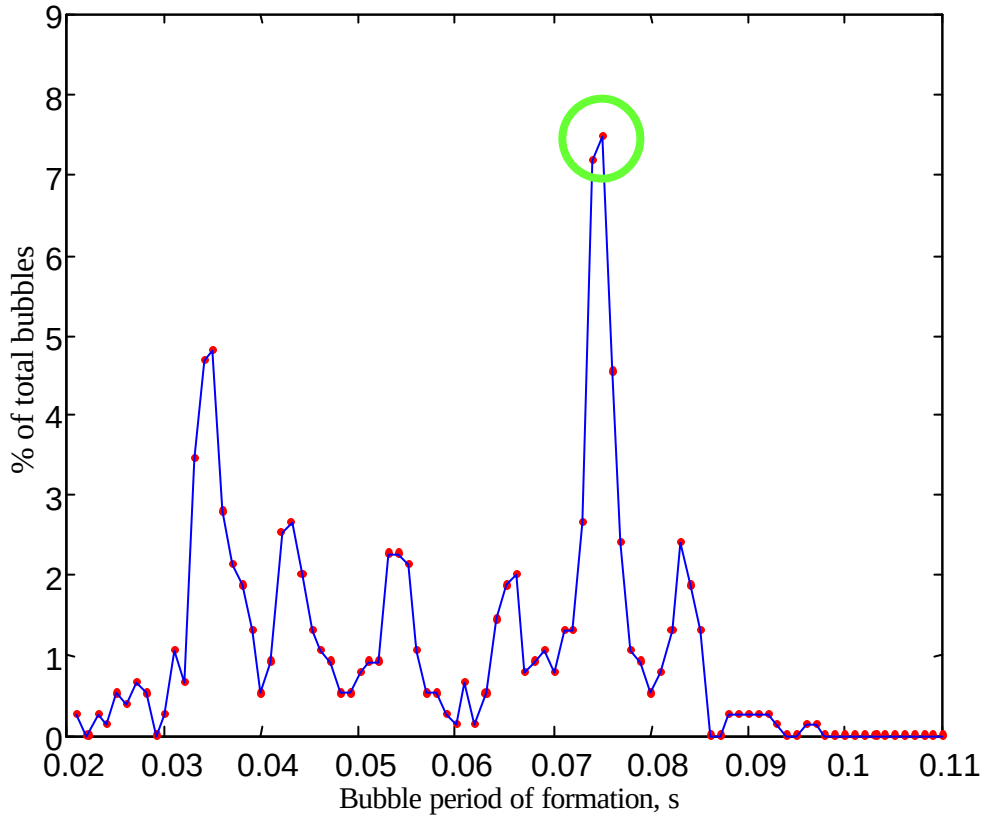

Figure 5.14. Frequency distribution of zero crossings after control is turned off (region d). Fixed-point hits decrease to 7.5% of the total number of bubbles

was observed in the pattern of the bubbles. This confirmed that the available gain was not sufficient to control the bubbling from chaotic bubbling to period-1. The present voltage swing available moves the fixed point by a distance of 0.001s. This is confirmed by the value of the shift vector which is 1e-5 s/volts. To move the fixed point by a distance of 0.01s, rather than 0.001s, an amplification factor of 10x is required for the present voltage swing. This would approximately mean a voltage swing of ~5000V.

5.4. Summary

Real time identification of bubbling was attempted through statistical modeling techniques. Real time identification was shown to succeed for bubbling regimes of period-1 and period-2 with a scheme that compares the sizes of bubbles with a previous moving window history. Regimes of period-4 could not be identified mainly because of lack of faster computing resources and the sensitivity of the calculations to measurement errors. Electrostatic potential was harnessed to control bubbling to a constant average bubble period of formation as the set point, with an increase/decrease in the flow-rate as the disturbance. It was found that with changes in disturbance the regime of bubbling could be changed while maintaining a constant average bubbling rate. Electrostatic potential was also used as the control variable in the OGY chaos control algorithm to tame the chaos in bubbling with partial success.